Memoirs of the Graduate Schools of Engineering and System Informatics Kobe University
No. 7, pp. 17–20, 2015. doi:10.5047/gseku.e.2015.004

[Research Topics]

Surface Plasmon Enhanced Emission Rate in Silicon Quantum Dot-Decorated Gold Nanorods in Solution

Hiroshi SUGIMOTO[1], Minoru FUJII[1], Björn M. Reinhard[2], Luca Dal Negro[3]

[1]*Department of Electrical and Electronic Engineering, Graduate School of Engineering, Kobe University*
[2]*Department of Chemistry & Photonics Center, Boston University*
[3]*Department of Electrical and Computer Engineering & Photonics Center, Boston University,*

(Received January 28, 2016; Accepted January 28, 2016; Online published May 16, 2016)

Keywords: *Biophotonics, Silicon quantum dots, Surface plasmon, Composite, Colloid*

This article summarizes research activities of Hiroshi Sugimoto at the Photonics Center in Boston University under the sponsorship of "Premium Program" of Graduate School of Engineering, Kobe University (September 2014 – July 2015). The main results are published in ACS Photonics (Vol. 2, pp. 1298−1305 (2015), DOI: 10.1021/acsphotonics.5b00233) and are reproduced in this article with permission from ACS publications.

Colloidal silicon quantum dots (Si-QDs) have attracted research attention as nanoprobes for bio-imaging due to the prominent photoluminescence (PL) properties and biocompatibility. In this work, for the enhancement of photoluminescence efficiency of Si-QDs, we develop colloidal nanocomposites consisting of luminescent Si-QDs and gold (Au) nanorods by a facile synthesis process. We systematically investigate the structural and PL properties, and demonstrate significant enhancement of the spontaneous emission rate due to the surface plasmon resonance of Au nanorods. We also show that the emission from Si-QDs coupled to Au nanorods is highly polarized along the major axis of nanorods. The experimental results in combination with simulations of dipolar emission in the vicinity of Au nanorods indicate a ~3 times enhancement of the quantum efficiency. The Si-based active plasmonic-coupled nanocomposites developed in this work provide novel opportunities for biocompatible platforms that leverage nanoscale fluorescent probes for biosensing and bio-imaging device applications.

1. Introduction

Nanometer-sized semiconductor crystal, so-called semiconductor nanocrystals or quantum dots (QDs), exhibit bright and wavelength tunable photoluminescence (PL) due to the quantum confinement effects. In particular, colloidal dispersion of semiconductor QDs with high chemical stability in aqueous media and high photo-stability during long-term illumination have been expected to take the place of organic dyes as nanoprobes for bio-imaging applications.[1] High-quality cadmium (Cd) and lead (Pb) chalcogenide QDs are commercially available. However, the toxicity of these QDs raises concerns for applications in biology and demands focused efforts aiming at the development of alternative solutions.

Silicon (Si) QDs are the most promising alternatives to toxic Cd- and Pb-based QDs because of the compatibility with biological substances and the bio-degradability. Numerous efforts have been made to develop water-dispersible and highly luminescent Si-QDs for the biological applications.[2,3] However, development of such systems is still challenging due to the difficulty of synthesizing high quality Si-QDs with bright photoluminescence (PL) in biological transparent windows (700-1200 nm) and with colloidal stability in aqueous solution.

Recently, we have developed a new type of all-inorganic colloidal Si-QDs. The Si-QDs consist of a nanocrystalline Si core and heavily boron (B) and phosphorus (P) doped shell, which induces negative surface potential and stabilize QDs in aqueous solution. B and P codoped Si-QDs are well-dispersed in water and exhibit excellent pH- and photo-stability of the PL. The PL wavelength is tunable in a very wide wavelength range (700-1400 nm).[4]

A drawback of the Si-QDs is a relatively small PL efficiency compared to that of Cd- and Pb-based compound semiconductor QDs. A promising approach to overcome the problem is utilizing enhanced electric fields accompanied by the excitation of localized surface plasmon resonances (LSPR) of metal nanostructures. It is well known that the enhanced local electric field in the vicinity of plasmonic nanostructures results in an increase of the local density of photonic states (LDOS), which leads to the enhancement of the radiative decay rate of antenna-coupled emitters. This coupling effect boosts the quantum efficiency by overcoming the fast relaxation into non-radiative decay channels.

In this work, we present a facile synthesis route of colloidal Au nanorods decorated with Si-QDs. Detailed PL studies including decay time at different emission wavelengths show enhancement of the spontaneous emission rate in the absence of non-radiative quenching by properly tuning the separation between QDs and metallic nanorods. Furthermore, the PL from individual QD-nanorod composites exhibits the same polarization dependence as the light scattering of the longitudinal plasmon mode of Au nanorods. These results in combination with theoretical calculations of radiative and non-radiative rates based on the boundary element method

(BEM) enabled us to accurately quantify the PL enhancement of Si-QDs coupled to Au nanorods. This work demonstrates that Si-based plasmonic-coupled nanocomposites are a very promising platform for bio-compatible active device applications to sensing and spectroscopy.

2. Materials and Methods

Colloidal Si-QDs of two different sizes were prepared by the method described in detail elsewhere.[4] The average diameter of Si-QDs is 3.3±0.9 (see Figure 1(a) and (b)). The QDs are well-dispersed in water without organic ligands. Positively-charged polymer-coated Au nanorods (A12-40-750-POS) were purchased from Nanopartz Inc. (Loveland, CO) and used as received. A representative transmission electron microscope (TEM) image is shown presented in Figure 1(c) and (d). The average length and width of the nanorods were 131±8 and 57±5 nm, respectively. A uniform polymer layer can be seen in Figure 1(d). The average thickness of the polymer layer is 8 nm with a standard deviation of 30%, which plays a crucial role for plasmonic-coupling between QDs and nanorods

Colloidal Si-QDs prepared in this work are negatively charged (-25 mV in water at pH 7) and Au nanorods are positively charged (+35 mV in water at pH 7). Therefore, by mixing Si-QD solution (1×10^{16} QDs/mL) with concentrated Au nanorod solution (1.7×10^{10} nanorods/mL) for 2 days, QDs attach to the surface of the nanorods by the electrostatic interaction. The mixed solution was subjected to centrifugation to remove unattached QDs, and QDs-decorated Au nanorods were redispersed in DI water.

TEM observations (Tecnai Osiris, FEI) were performed for carbon-coated TEM meshes on which the solution containing Si-QD-decorated Au nanorods was drop-coated. Absorption spectra of QDs and nanorods were acquired with a spectrophotometer (CARY 5000, Varian). Dark-field scattering and PL images of composites were obtained using an inverted microscope (IX71, Olympus) equipped with a high-resolution electron multiplying charge coupled device (EMCCD) (iXonEM, Andor). For dark-field measurements, the samples were illuminated through an air dark-field condenser. To obtain PL images, a 100 W mercury lamp (U-LH100HG, Olympus) with 10 nm bandpass filter centered at 430 nm was used as an excitation source. The excitation light was filtered using a proper long pass filter and only emission from composites was detected by CCD. In this condition, Au nanorods without Si-QDs do not show any PL in the images. Polarization-dependence of scattering and PL images were taken with a polarization analyzer placed in front of the detector. PL spectra and decay dynamics were measured using a monochromator (Oriel Cornerstone 260, Newport) and photomultiplier tubes for visible (Oriel 77348, Newport) and near-IR (R5509-73, Hamamatsu) regions. The excitation source was electrically-modulated light from laser diode of 405 nm (IQ1A-100, Power Technology Inc.). All the measurements were carried out at room temperature.

3. Results and Discussion

Figure 1(e) summarizes the optical properties of Si-QDs and Au nanorods in water. The QDs exhibit a broad PL spectrum peaked at 750 nm. The scattering peak of longitudinal LSPR of Au nanorods at 750 nm overlaps with the PL spectrum of QDs. The weak transverse mode is also observed at 525 nm.

Figure 2(a) shows a representative TEM image of a single Au nanorod decorated with Si-QDs that are attached on the surface of the nanorod by electrostatic attraction in solution. In the high-resolution TEM image in Figure 2(b), the lattice fringes corresponding to {111} planes of Si crystal can be clearly observed. These images demonstrate that single-crystalline Si-QDs are attached to the Au nanorods. The average separation between QDs and nanorods estimated by inspecting several TEM images is 8.7 nm.

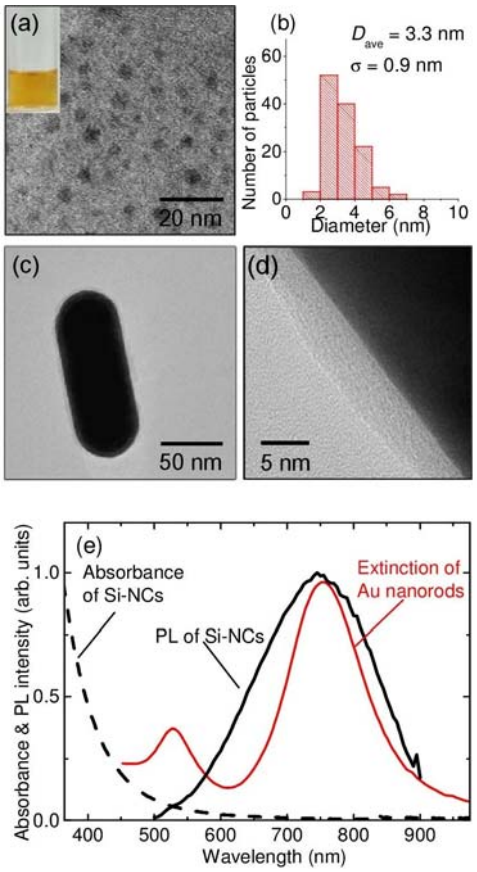

Fig. 1 (a) Photograph and TEM image of Si-QDs and (b) the size distribution. (c), (d) TEM images of a positively-charged polymer coated Au nanorod. (e) Absorbance (dashed) and normalized PL spectra (solid) of Si-QDs and extinction spectrum of Au nanorods (red). Reproduced with permission from *H. Sugimoto, et al., ACS Photonics, 2, 1298−1305 (2015).* Copyright 2015, American Chemical Society.

Figure 2(c) displays a normalized PL spectrum of Au nanorods decorated with Si-QDs. We also plot the PL spectrum of reference (Si-QDs without nanorods in water) and the extinction spectrum of Au nanorods. We do not observe a dramatic change of the PL spectral shape by the coupling with Au nanorods. To investigate the spontaneous emission rate of QDs coupled to Au nanorods, we measure the PL decay curves in a wide wavelength range. The PL decay curves of Si-QDs are not a single-exponential function. In this work, a stretched exponential function, $I = I_0 exp[-(t/\tau)]^{\beta}$, where τ is the measurable decay constant and β is the stretching parameter of the decay, is used to estimate the lifetime of Si-QDs. The fitted β values vary from 0.55 to 0.85 for QDs coupled to nanorod, indicating a significant distribution of decay rates for each emission wavelength. According to the stretched exponential theory, an average lifetime can be defined as $\tau_{ave} = \tau\ \beta^{-1}\ \Gamma(\beta^{-1})$, where Γ is the Euler gamma function.[6] We approximate the decay rate with $\Gamma_{ave} = \tau_{ave}^{-1}$ and calculate the enhancement factors by

considering the ratio of decay rates of QDs with and without Au nanorods. The decay rate enhancements are shown in Figure 2(d), which shows a clear dependence on the emission wavelength. The maximum enhancement reaches approximately 1.4. The enhancement factor is larger at the wavelengths of the longitudinal LSPR mode of the nanorods. In Figure 2(d), at emission wavelengths on both sides of the peak, the decay rate enhancement factor approaches unity. This indicates that, irrespective of wavelength, the non-radiative energy transfer commonly observed for emitters positioned very close to metal (2-5 nm) surfaces[7,8] is suppressed by the presence of the polymer spacer layer. We performed the same measurements for Si-QD-decorated Au nanorods using a thinner polymer layer. In this case, the decay rate enhancement is approximately 3.5 for the overall PL spectrum. This proves that non-radiative decay channels are dominant for this sample.

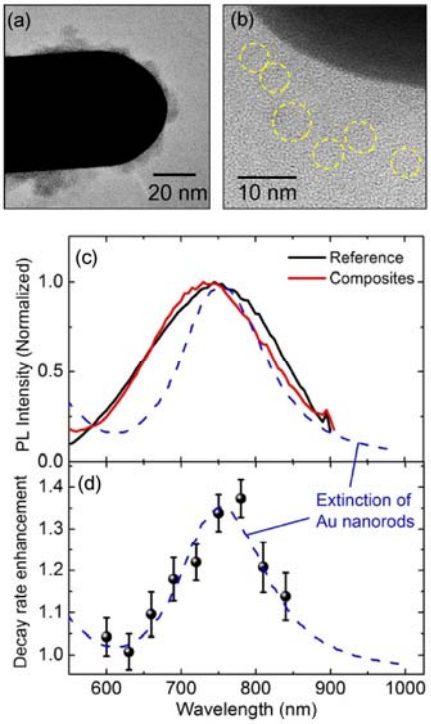

Fig. 2 (a) TEM image of Au nanorods decorated with Si-QDs. (b) High-resolution TEM image of a composite. Single-crystalline Si-QDs are attached to a nanorod surface with separation by polymer spacer. (c) Normalized PL spectra of Si-QDs coupled with Au nanorods (red line) and QDs alone (black line). (d) Decay rate enhancement of Si-QDs coupled with Au nanorods as a function of emission wavelength. The error bars include the error during the fitting process. Reproduced with permission from *H. Sugimoto, et al., ACS Photonics, 2, 1298−1305 (2015).* Copyright 2015, American Chemical Society.

To study the coupling between QDs and Au nanorods more in detail, we measure the PL polarization properties. Figure 3(a) shows the polar plots of the dark-field scattering intensities of a representative composite as a function of the analyzer angles. Since the strong dipolar LSPR of Au nanorods is inherently polarized along their major axis (longitudinal mode), the scattered light from the nanorod is also linearly polarized along the major axis.[9] Figure 3(b) shows the polar plots of PL intensities of the same nanocomposite (red). The PL from QDs attached to the nanorod is also highly polarized along the major axis of the nanorod. We observe similar features for several spots in different areas. The linearly polarized emission from randomly oriented emitters coupled to metal nanostructures has been reported for Au nanorods coated with dye-doped silica shells.[9] Note that the PL from an "ensemble" of QDs is expected to be unpolarized due to the random orientation of the QDs. In Figure 3(b), we confirm this by comparing the polarized emission of Si-QDs coupled and uncoupled to Au nanorods. The linearly polarized PL from nanocomposites reflects the PL enhancement of Si-QDs due to the plasmon coupling with longitudinal modes of Au nanorods.

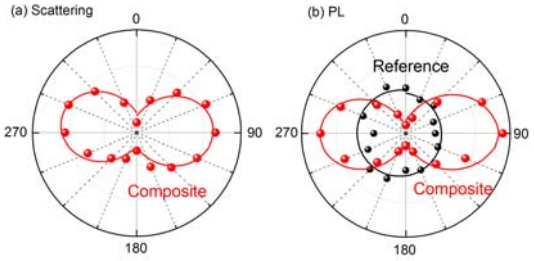

Fig. 3 Polar plots of (a) dark-field scattering and (b) PL intensities of nanocomposites (red) and ensemble Si-QDs without Au nanorod (black) as a function of polarization angles. Reproduced with permission from *H. Sugimoto, et al., ACS Photonics, 2, 1298−1305 (2015).* Copyright 2015, American Chemical Society.

The enhancement of spontaneous emission rate in Figure 2 is explained by the enhancement of LDOS due to the LSPR of Au nanorods. To discuss the contribution of the radiative and non-radiative rates to the quantum efficiency of Si QDs-decorated Au nanorods, we performed theoretical calculations using the MNPBEM code,[10] which is based on the rigorous boundary element method. The decay rates in the vicinity of Au nanorod with the diameter of 60 nm and the length of 126 nm have been simulated by placing point dipoles at fixed distances from the nanorod surface with tabulated dispersion data.[11] The results are normalized by the emission rate of a dipole in water, and thus we use the term radiative and non-radiative rate enhancements to describe the modification of decay rate due to the presence of a Au nanorod.

In order to quantitatively determine the quantum efficiency enhancement, we now combine experimental and theoretical results. We focus on the wavelength at 750 nm (Peaks of QD PL and nanorod scattering). The intrinsic quantum efficiency (Q_0) of Si-QDs is expressed as $Q_0 = \gamma_r^0/(\gamma_r^0 + \gamma_{nr}^0)$, where γ_r^0 and γ_{nr}^0 are the intrinsic radiative and non-radiative decay rates of QDs in aqueous solution. The modified quantum efficiency of QDs by the coupling with Au nanorods (Q_m) is defined by

$$Q_m = \Gamma_r / (\Gamma_r + \Gamma_{abs} + \gamma_{nr}^0) \quad (1).$$

Here, Γ_r is the modified radiative rate, and Γ_r/γ_r^0 corresponds to the Purcell factor[12,13] with respect to the emission of a dipole in water and Γ_{abs} is the plasmon-induced non-radiative rate due to the absorption by the metallic nanorods. In Eq (1), we assume that only the radiative rate is modified by the coupling with Au nanorods because the intrinsic non-radiative rate (γ_{nr}^0) arising from material imperfections of Si-QDs is not affected by the local electromagnetic environment.[14] In fact, the decay rate

enhancement shown in Figure 2(d) is almost unity at wavelengths that are detuned from the resonance of Au nanorods. This confirms that the measured decay rate enhancement is due to Γ_r/γ_r^0 (Purcell enhancement) and Γ_{abs}/γ_r^0 (absorption by Au nanorods) rather than modification of internal non-radiative rate of Si-QDs by coupling with nanorods.

Total decay rate enhancement (W_{exp}) shown in Figure 2(d) can be expressed by $W_{exp} = (\Gamma_r + \Gamma_{abs} + \gamma_{nr}^0) / (\gamma_r^0 + \gamma_{nr}^0)$. By combining the experimentally obtained W_{exp} with the Γ_r/γ_r^0 and Γ_{abs}/γ_r^0 values obtained from the simulations, we can calculate Q_0, Q_m and the enhancement of the quantum efficiency of Si QDs from the relation between them ($Q_m/Q_0 = (\Gamma_r/\gamma_r^0) / W_{exp}$). In Table 1, we summarize the results at 750 nm (the QD PL peak). By coupling with Au nanorods, the quantum efficiency of QD emission is enhanced by a factor of 2.8. We notice that this large enhancement is achieved only by engineering the radiative decay rate without the contribution from excitation enhancement (pumping enhancement). We also observe that the calculated Q_0 is in excellent agreement with measured PL quantum yield (6.9±0.7%) of our Si-QDs in water,[15] which proves the validity of our analysis.

Table 1. Parameters of emission of Si-QDs at 750 nm. Measured total decay rate enhancement (W_{exp}), radiative (Γ_r/γ_r^0) and non-radiative (Γ_{abs}/γ_r^0) decay rate enhancements from simulation, calculated intrinsic (Q_0) and modified (Q_m) quantum effciencies, and calculated quantum efficiency enehancement. Reproduced with permission from *H. Sugimoto, et al., ACS Photonics, 2, 1298−1305 (2015).* Copyright 2015, American Chemical Society.

λ(nm)	W_{exp}	Γ_r/γ_r^0	Γ_{abs}/γ_r^0	Q_0 (%)	Q_m (%)
750	1.35	3.77	2.23	7.4	20.7

4. Conclusion

We have developed a novel plasmon-coupled fluorescent platform based on Au nanorods decorated with Si-QDs. Through PL decay dynamics measurements performed over a wide wavelength range, we have shown enhanced decay rates that follow the LSPR scattering spectrum of nanorods. The PL imaging and scattering maps of individual nanocomposites demonstrate that the polarized PL of Si-QDs is driven by the efficient excitation of the longitudinal mode of Au nanorods. From a systematic PL analysis performed in partnership with theoretical calculations, we demonstrated a quantum efficiency enhancement of Si-QDs up to approximately a factor of 3. Si-based plasmon-coupled nanocomposites prepared by facile and cost-effective method are very promising candidates for the development of biocompatible fluorescent nanoprobes of interest to biosensing and bio-imaging technologies.

References

(1) Medintz, I. L.; Uyeda, H. T.; Goldman, E. R.; Mattoussi, H. Quantum Dot Bioconjugates for Imaging, Labelling and Sensing. *Nat. Mater.* **2005**, *4*, 435–446.

(2) Li, Z. F.; Ruckenstein, E. Water-Soluble Poly(acrylic Acid) Grafted Luminescent Silicon Nanoparticles and Their Use as Fluorescent Biological Staining Labels. *Nano Lett.* **2004**, *4*, 1463–1467.

(3) Erogbogbo, F.; Chang, C.; Yong, K.; Law, W.; Ding, H.; Roy, I.; Swihart, M. T.; Prasad, P. N. 2011 Bioconjugation of Luminescent Silicon Quantum Dots for Selective.pdf. **2011**, 1081–1088.

(4) Sugimoto, H.; Fujii, M.; Imakita, K.; Hayashi, S.; Akamatsu, K. Codoping N- and P-Type Impurities in Colloidal Silicon Nanocrystals: Controlling Luminescence Energy from below Bulk Band Gap to Visible Range. *J. Phys. Chem. C* **2013**, *117*, 11850–11857.

(5) Linnros, J.; Lalic, N.; Galeckas, A.; Grivickas, V. Analysis of the Stretched Exponential Photoluminescence Decay from Nanometer-Sized Silicon Crystals in SiO[sub 2]. *J. Appl. Phys.* **1999**, *86*, 6128.

(6) Lindsey, C. P.; Patterson, G. D. Detailed Comparison of the Williams–Watts and Cole–Davidson Functions. *J. Chem. Phys.* **1980**, *73*, 3348.

(7) Viste, P.; Plain, J.; Jaffiol, R.; Vial, A.; Adam, P. M.; Royer, P. Enhancement and Quenching Regimes in Metal-Semiconductor Hybrid Optical Nanosources. *ACS Nano* **2010**, *4*, 759–764.

(8) Munechika, K.; Chen, Y.; Tillack, A. F.; Kulkarni, A. P.; Plante, I. J. La; Munro, A. M.; Ginger, D. S. Spectral Control of Plasmonic Emission Enhancement from Quantum Dots near Single Silver Nanoprisms. *Nano Lett.* **2010**, *10*, 2598–2603.

(9) Ming, T.; Zhao, L.; Chen, H.; Woo, K. C.; Wang, J.; Lin, H. Experimental Evidence of Plasmophores: Plasmon-Directed Polarized Emission from Gold Nanorod–Fluorophore Hybrid Nanostructures. *Nano Lett.* **2011**, *11*, 2296–2303.

(10) Hohenester, U.; Trügler, A. MNPBEM - A Matlab Toolbox for the Simulation of Plasmonic Nanoparticles. *Comput. Phys. Commun.* **2012**, *183*, 370–381.

(11) Johnson Christy, R. W., P. B. Optical Constants of the Noble Metals. *Physical Review B*, 1972, *6*, 4370–4379.

(12) Purcell, E. M. Spontaneous Emission Probabliities at Radio Frquencies. *Phys. Rev.* **1946**, *69*, 674–674.

(13) Akselrod, G. M.; Argyropoulos, C.; Hoang, T. B.; Ciracì, C.; Fang, C.; Huang, J.; Smith, D. R.; Mikkelsen, M. H. Probing the Mechanisms of Large Purcell Enhancement in Plasmonic Nanoantennas. *Nat. Photonics* **2014**, *8*, 1–15.

(14) Govorov, A. O.; Bryant, G. W.; Zhang, W.; Skeini, T.; Lee, J.; Kotov, N. a; Slocik, J. M.; Naik, R. R. Exciton Plasmon Interaction and Hybrid Excitons in Semiconductor Metal Nanoparticle Assemblies. *Nano Lett.* **2006**, *6*, 984–994.

(15) Sugimoto, H.; Fujii, M.; Fukuda, Y.; Imakita, K.; Akamatsu, K. All-Inorganic Water-Dispersible Silicon Quantum Dots: Highly Efficient near-Infrared Luminescence in a Wide pH Range. *Nanoscale* **2014**, *6*, 122–126.